RESEARCH PAPER

Development And Optimization Of Resveratrol Loaded Nanosuspension Using Central Composite Design (Ccd) For Age Related Macular Degeneration Disease

Pradeep Kumar Singh[1*], Komal Patel[2], Neelkant Prasad[3], Vivek Yadav[4]

[1] Department Of Pharmaceutics, Faculty Of Pharmacy, Parul University, Waghodia, Vadodara, Gujarat, 391760, India. Orcid: 0009-0006-2949-4448

[2] Department Of Pharmacognosy, Parul Institute Of Pharmacy, Faculty Of Pharmacy, Parul University, Waghodia, Vadodara, Gujarat, 391760, India. Orcid: 0000-0003-1077-2584

[3] Sgt College Of Pharmacy, Sgt University, Gurugram-Badli Road, Budhera, Gurugram, Haryana, India-122505. Orcid: 0000-0002-8333-8810

[4] Department Of Pharmaceutics, School Of Pharmaceutical Education And Research, Jamia Hamdard, New Delhi, India, 110062. Orcid: 0009-0008-3730-5736

Corresponding Author: Pradeep Kumar Singh, Ph. D. Scholar (Research Scholar), Department Of Pharmaceutics, Faculty Of Pharmacy, Parul University, Waghodia, Vadodara, Gujarat, 391760, India. Email: pradeepsingh414@gmail.com

Received: *20th Feb, 2026;* ***Revised:*** *4th Mar, 2026;* ***Accepted:*** *25th Mar, 2026;* ***Available Online:*** *10th Apr, 2026*

Abstract

Background: Resveratrol (res) exhibits potent antioxidant and anti-inflammatory activities that are relevant for the treatment of age-related macular degeneration (amd). However, its poor solubility and low ocular bioavailability significantly limit its clinical translation.

Objective: To develop an ophthalmic res suspension (or nanosuspension) and optimize the formulation and process variables using central composite design (ccd) within a quality by design (qbd) framework.

Methods: A rotatable three factor ccd was employed to study the effects of (a) stabilizer concentration of plga (mg) 30-50 / pva (%), 1–1.50 w/w, (b) homogenization speed (10–25 krpm) on critical quality attributes (cqas): particle size, pdi, zeta potential and in vitro release. Responses were modeled by second order polynomials; model adequacy was evaluated by anova, lack of fit, and diagnostic plots. Desirability based multi response optimization yielded a design space targeting minimized size (105.2 nm) / pdi (0.254), acceptable zeta potential (-40 mv), ocular ph (6.5–7.8), and viscosity suitable for drops.

Results: Ftir and dsc results show no drug-excipients interaction. The particle size and pdi of the optimized preparation had the values of 122.5 nm and 0.36, respectively. -40.0 ± 4.19 mv value of zeta potential indicates that the optimized formulation will be sufficiently stable. Entrapment efficiency was also found to be good i.e. 75.200%. Dpph assay revealed a good free radical scavenging capability of the optimized formulation which was found to be comparable with ascorbic acid as standard and better than res solution.

Conclusion: Central composite design (ccd) efficiently mapped the formulation-process space and optimized an ocularly compatible resveratrol (res) suspension with enhanced biopharmaceutical properties for effective age-related macular degeneration management.

Keywords: Resveratrol, Amd, Ophthalmic Suspension, Nanosuspension, Quality By Design, Central Composite Design, Response Surface Methodology, Ocular Delivery.

How To Cite This Article: Singh Pk, Patel K, Prasad N, Yadav V. Development And Optimization Of Resveratrol Loaded Nanosuspension Using Central Composite Design (Ccd) For Age Related Macular Degeneration Disease. Int J Drug Deliv Technol. 2026;16(26s):249-265. Doi: 10.25258/ijddt.16.26s.25

INTRODUCTION

Age-Related Macular Degeneration (AMD) is a progressive disorder of the macula that leads to vision loss, primarily affecting elderly patients. The macula, located in the retina, is responsible for central visual acuity and color vision[1,2]. AMD causes visual impairment along with psychological effects such as anxiety, depression, and emotional distress. The condition results from degeneration of retinal pigment epithelium (RPE) cells and light-sensitive photoreceptor cells[1,2]. AMD mainly exists in two forms: exudative choroidal neovascularization (CNV)

and dry geographic atrophy (GA)[1,2]. Global AMD cases are projected to reach approximately 288 million by 2040[3]. Vision loss in AMD due to CNV is driven by the proangiogenic cytokine vascular endothelial growth factor (VEGF). Current pharmacological interventions include VEGF inhibitors such as bevacizumab (Avastin), aflibercept (Eylea), and pegaptanib (Macugen)[4]. However, ocular drug delivery poses significant challenges in targeting the posterior eye segment[5], especially for drugs with poor and inconsistent solubility. Most AMD therapeutics are administered via intravitreal injections, which are expensive and often associated with adverse effects such as cataracts, elevated intraocular pressure, and endophthalmitis, in addition to requiring repeated invasive administration[6-11]. These challenges highlight the unmet need for alternative, cost-effective therapies.

Resveratrol (RES), chemically known as 3,5,4′-trihydroxy-trans-stilbene, is a natural polyphenolic compound found in grapes and red wine[12,13]. Due to its potent antioxidant and anti-inflammatory properties, RES shows promise as a neuroprotective, cardio-protective, anti-aging, and chemotherapeutic agent[14,15]. Research indicates that RES prevents oxidative stress-induced apoptosis in human RPE cells by suppressing reactive oxygen species (ROS) production[16]. Clinical studies (e.g., NCT02625376) are ongoing to evaluate RES as a food supplement for AMD management[11]. RES reduces pathological neovascularization by inhibiting hypoxia-induced expression of VEGF, mainly through suppression of transcription factors HIF-1α and NFκB[17,18]. Despite its potential, RES suffers from poor aqueous solubility and low bioavailability, which restrict its clinical translation. To overcome these challenges, research is focused on developing formulations that provide localized, sustained action, minimize repeated dosing, and reduce systemic adverse effects[19]. Nanosuspensions, consisting of nano-sized drug particles stabilized in surfactant solutions or polymeric nano-encapsulated drug reservoirs, offer promising solutions for ocular drug delivery. Nanoparticles facilitate prolonged drug residence time in the ocular microenvironment and enable drug permeation through ocular barriers to the posterior segment[20,21]. Their small size enhances solubility, absorption, and pharmacokinetics of poorly soluble drugs[22]. For formulation optimization, Central Composite Design (CCD) under Response Surface Methodology (RSM) is highly suitable. CCD organizes experiments with cube points, center points, and axial points in a wedge arrangement—rotational or orthogonal—to predict variable interactions and minimize regression variability[23-26]. First introduced by Box and Hunter, RSM allows for polynomial or quadratic modeling of formulation-process variables[24,27-30].

In this study, a PLGA polymer-based nanosuspension was developed as a carrier system for ocular delivery of resveratrol. Given its reported antioxidant and anti-VEGF activity, we aimed to formulate a nanosuspension to enhance therapeutic outcomes in AMD treatment.
The resveratrol nanosuspensions were prepared via solvent evaporation[31] and formulation-process parameters were optimized using CCD to achieve minimal particle size, maximal drug encapsulation, and sustained release. The optimized formulation was further evaluated for antioxidant activity, which plays a crucial role in mitigating AMD progression.

MATERIALS AND METHODS

Materials

Resveratrol, polyvinyl alcohol and PLGA (50-50) were got from Sigma-Aldrich, Mumbai, India. Acetone was got from SRL Chem Pvt. Ltd., Indore, India. Tween 80 was purchased from Fisher Scientific, Mumbai, India. Dialysis membrane (molecular weight cut-off 12 kDa) was purchased from Himedia, Mumbai, India. All other chemicals, reagents were of analytical grade.

Methods

Preparation of RES Nanosuspension

RES-loaded nanosuspension was prepared by the solvent evaporation method. Accurately weighed 40 mg of PLGA was solubilized in 10 ml acetone followed by dissolution of 2.5 mg of RES in this solution. The solution, thus prepared, was then progressively added to the 1.5% w/v aqueous solution of PVA at ambient temperature (25˚C). The mixture was then probe sonicated for 1 minute followed by magnetic stirring at 1650 rpm till thorough evaporation of the organic solvent. The resulting nanoparticle dispersion was then frizzed and lyophilized using as cryoprotectant (1% w/v mannitol solution) to get nano-suspension[32].

Optimization of RES Nanosuspension by Central Composite Design

The CCD generated 13 experimental trial formulations (**Table 1**) using Design Expert 9.0.4.1

software (Stat-Ease, Minnesota, USA). Two formulation variables having three levels, namely Factor 1 i.e. PLGA and Factor 2 i.e. PVA, were used keeping rest of the elements including RES constant. RSM was cast-off to assess the impact of independent variables (i.e. factors) on dependent variables (i.e. responses) comprising particle size (Y1), polydispersity index (Y2), and entrapment efficiency (Y3). Several levels of variables are presented in **Table 1**. The coded and actual factors of the design of experiments are expressed in **Table 2**.

Table 1: Levels of variables for optimization

Code	Variables	Levels of Variables				
		-1	**0**	**+1**	**-α**	**+α**
Factor 1	PLGA (mg)	30	40	50	25.8579	54.1421
Factor 2	PVA (%)	1	1.5	2	0.792893	2.20711

Table 2: Formulation composition for optimization of RES nanosuspension as per CCD

Standard	Run Order	Factor 1 (A: PLGA)		Factor 2 (B: PVA)	
		Coded Values	Actual Values (mg)	Coded Values	Actual Values (%)
6	1	+α	54.1421	0	1.5
4	2	+1	50	+1	2
1	3	-1	30	-1	1
2	4	+1	50	-1	1
11	5	0	40	0	1.5
7	6	0	40	-α	0. 792893
10	7	0	40	0	1.5
5	8	-α	25.8579	0	1.5
8	9	0	40	+α	2.20711
3	10	-1	30	+1	2
9	11	0	40	0	1.5
13	12	0	40	0	1.5
12	13	0	40	0	1.5

The RSM was applied for optimization[33-35]. **Tables 1** and **2** represents the details of the dependent and independent variables. The data obtained for CQAs i.e. particle size (Y), PDI (Y2), and entrapment efficiency (Y3) of RES nanosuspension was subjected to mathematical modelling for establishing suitable polynomial models with the studied factors. The best fitted model was identified via statistical strictures such as regression coefficient (r^2), coefficient of variance (% CV), adjusted and predicted r^2 and "predicted residual error sum of squares" (PRESS) for different investigated models for the CQAs. The impact of independent variables on responses was studied through 2D-contour plots and 3D-response surface graphs. Based on model fitting for each of the response variables, optimum design was picked by numerical and graphical search methods. In numerical search, acceptable ranges of the CQAs were defined and weightage was given for selecting optimized formulation based on the desirability value closer to 1. Based on the ranges of CQAs assigned in numerical search, graphical optimization was done to demarcate the design space and locating the optimized formulation within the design space[36-38].

The RSM was chosen for optimization in the current study[33-35]. Thirteen formulations were created and their response variables i.e. particle size, PDI, and entrapment efficiency were assessed. The correlations between all the factors and the response variables were investigated using quadratic models. **Table 3** displays the summary of the statistical model for the response variables. To examine the difference between the fitted and obtained values, the lack of fit test is used. Additionally, r^2 value of the responses and the substantial lack of fit were calculated.

Table 3: Formulations designed for optimization of RES nanosuspension using central composite design

Std.	Run Order	Factor 1 (A: PLGA)		Factor 2 (B: PVA)	
		Coded Values	Actual Value (mg)	Coded Values	Actual Values (%)
6	1	+α	54.1421	0	1.5
4	2	+1	50	+1	2
1	3	-1	30	-1	1
2	4	+1	50	-1	1
11	5	0	40	0	1.5
7	6	0	40	-α	0.792893
10	7	0	40	0	1.5
5	8	-α	25.8579	0	1.5
8	9	0	40	+α	2.20711
3	10	-1	30	+1	2
9	11	0	40	0	1.5
13	12	0	40	0	1.5
12	13	0	40	0	1.5

Characterization of RES nanosuspension

Physicochemical characterization

RES nanosuspensions were estimated for physicochemical parameters by DSC and FTIR spectroscopy[39]. FTIR spectroscopy was performed to evaluate the chemical structure of resveratrol (RES),

identify characteristic functional groups, assess potential incompatibilities with excipients, and confirm the successful incorporation of RES into the nanosuspensions. The FTIR spectra of RES alone, RES-PLGA physical mixture, RES-PVA physical mixture, and RES nanosuspension were recorded in the range of 4000 cm^{-1} to 400 cm^{-1} and compared with the reference standard of pure RES to investigate possible drug-excipient interactions.

Differential Scanning Calorimetry (DSC) analysis was performed for RES alone, RES-PLGA physical mixture, RES-PVA physical mixture, and RES nanosuspension. Approximately 5 mg of each sample was placed in a sealed DSC pan and heated from 30°C to 400°C at a rate of 10°C/min under nitrogen atmosphere with a flow rate of 50 ml/min. An empty aluminum pan was used as the reference. This analysis provided insight into the thermal behaviour and drug-excipients compatibility as well as the physical state of RES in the nanosuspension[40].

Transmission Electron Microscopy (TEM)

TEM was performed to evaluate the surface characteristics of the sample. The surface characteristics was obtained when a beam of electrons was transmitted through an ultra-thin sample, interacting with the sample as it passed through it[41]. Transmission electron microscopy (TEM-Tecnai, G20, Philips scientific, Netherlands) was used for morphological analysis of optimized formulation. A drop of diluted sample was taken on a copper grid and allowed to get dry then stained with 1% phosphotungstic acid[42].

Particle size, polydispersity index and zeta potential

1 ml Aliquots of RES nanosuspension dispersions were diluted 100-fold with distilled water for measurement of particle size and PDI as well as zeta potential by "dynamic light scattering" (DLS) technique (Nano ZS90, Malvern Panalytical, UK)[43]. The formulation was 100 times diluted with filtered distilled water followed by analysing in triplicate at 25°C for particle size and PDI. Zeta potential was measured using same device in a zeta cuvette after 100-fold dilution of the formulation with filtered distilled water[44].

Entrapment efficiency

To find out the entrapment efficiency of RES nanosuspension, 0.5 ml of the nanosuspension was subjected to ultra-centrifugation at 10,000 rpm (2,236×g i.e.10 kDa) in Amicon centrifuge tubes (Milipore, Mumbai, India) to remove unentrapped drug, if any, and pellet down the nanoparticles followed by dissolution of pelleted nanoparticles in methanol to extract out RES. The quantity of entrapped drug was then enumerated by spectrophotometry at 306 nm and the entrapment efficiency was determined by the formula given below[41]-

$$\text{Entrapment Efficiency} = \frac{\text{Actual Amount of the Drug Loaded in Nanosuspensions}}{\text{Actual Amount of the Drug Used for Preparation of Nanosuspensions}} \times 100$$

***In vitro* drug release studies of optimized RES nanosuspension**

In vitro drug release from the optimized RES nanosuspension was planned in six replicates to compare the release of RES from RES solution and RES nanosuspensions at 37°C±0.5°C using dialysis bag (12 kDa) in 100 ml of phosphate buffer pH 7.4 having 0.1% v/v of Tween 80 for up to 24 hours at 100 RPM[45]. RES nanosuspension having 0.5 mg/0.5 ml RES was filled in dialysis bag and tied on its both ends. Samples (3 ml) were taken out at 0, 0.5, 1, 2, 4, 6, 8, 10, 12, 16, 20, 24 hours subsequently replacing with the equal volume of fresh medium to conserve sink conditions. The drug release was quantified at 306 nm using UV spectrophotometry after suitable dilution. The results were presented as cumulative per cent drug released at predetermined time points versus time curve (Release Profile)[46].

DPPH antioxidant assay

The free radical scavenging activity of the optimized RES nanosuspension was verified using a 1,1-diphenyl2-picrylhydrazyl (DPPH) assay. 24 mg DPPH was dissolved in methanol to get 100 ml stock solution. The later was then filtered to get a filtrate as DPPH working solution (Blank) having light absorbance nearly 0.973 at 517 nm. A test tube was filled with 100 µl of the test formulation and 3 ml of DPPH working solutions. The tubes were then left in complete dark for half an hour. Thus, a wavelength of 517 nm was used to estimate the absorbance. The following formula was used to compute the percentage scavenging[47,48].

$$\%\ \textbf{Scavenging} = \frac{(\textbf{Absorbance of Blank}_{517} - \textbf{Absorbance of Sample}_{517})}{\textbf{Absorbance of Blank}_{517}}$$

Age Related Macular Degeneration Studies in Animals

Albino rabbits, which were of trust to pharmacological treatments and experimentation,

weighing 2.5-3.0 kg and at least 4 months of age, were used. The animals were held in groups of one per cage and kept in standard conditions at 25±2 °C temperature, 55±5% humidity and light and dark cycle of 12 hours each. The animals have limitless access to tap water and rodent food. The protocol was duly approved from the Institutional Animal Ethics Committee vide protocol number **AIPS/IAEC/02/12**, which was established to oversee and manage experimental animals and adhere to the widely accepted Principles for Laboratory Animal Use and Care as stated in the National Institutes of Health Guide (NIH Publication No. 85-23, revised 1985)[49]. Every test was carried out from 9:00 hours to 18:00 hours.

In this study, a sodium iodate ($NaIO_3$)-induced dry age-related macular degeneration (AMD) model was used. In harmony with a prior method, IV injection of $NaIO_3$ (30 mg/kg) was used to demonstrate oxidative stress-mediated degeneration in the retina and retinal pigment epithelia (RPE)[50]. Animals (n=3) were divided into five groups i.e. normal group, disease group, free RES treated group (20 mg/kg), RES nanosuspension treated group (equivalent to 20 mg/kg RES), and bevacizumab (1.25 mg) treated standard group. The normal group of rabbits received physiological saline intravitreally, whereas the other groups received injections of 30 mg/kg $NaIO_3$. The matching preparations were administered four times a day starting the following day. The literature provided the dose of RES[51].

The altered Draize test[52] was used to conduct eye irritation test. Each rabbit's ocular situations were examined in order to gauge irritation. The rabbits were put to sleep after receiving the medication four times a day for 28 days straight. The eyeballs were then promptly removed and a homogenate was made. This homogenate was used for further biochemical assessment.

Assessment of Oxidative Stress

Measurement of lipid peroxidation

Malondialdehyde (MDA) content was measured as an estimate lipid peroxidation using the previously pronounced method by Ohkawa et al. (1979)[53] with a minimal adjustment. In short, 1.5 ml glacial acetic acid (20%), 0.2 ml sodium dodecyl sulphate (8.1%), and 1.5 ml thiobarbituric acid (0.8%) were combined with the 0.1 ml eye homogenate sample. The tube-containing mixture was stirred, heated on a water bath for one hour at 95 °C, and then cooled below running water. Each tube was then filled with 5 ml of pyridine and n-butanol (1:15) and 1 ml of distilled water, and the tubes were centrifuged for 10 minutes at 4000 rpm. To assess the amount of MDA produced, the absorbance of the upper organic pink layer was measured at 532 nm. A calibration curve was generated using malondialdehyde bis-(dimethoxy acetyl) as the standard. The data were stated as nmol of MDA/mg protein[54].

Measurement of Glutathione

The valuation of glutathione (GSH) was done using Ellman's (1959) methodology[55]. In short, 2 ml of Ellman's reagent (5'5 dithiobis [2-nitrobenzoic acid] 10 mM and NaHCO3 15 mM) were combined with 160 µl of homogenate. The absorbance at 412 nm was measured after the mixture-containing tubes were incubated for five minutes at room temperature. The activity was expressed in µmol/mg of protein[56].

Measurement of Inflammatory Cytokines (TNF-α and IL-6)

The murine TNF-α and IL-6 immunoassay kits were used to quantify TNF-α and IL-6. Using a pre-coated murine-specific monoclonal antibody and a supplied murine-specific enzyme-linked polyclonal antibody for TNF-α and IL-6, the sandwich ELISA procedure has been used for control, standard or test samples. In part to the quantity of murine TNF-α and IL-6 bound in the first steps, the colour intensity was assessed at 450 nm as the primary wavelength and 620 nm as the reference wavelength. The standard curve was then used to read off the sample data[57].

Measurement of VEGF for Angiogenesis

As directed by the manufacturer, the human VEGF-A ELISA Kit was cast-off to measure the VEGF protein in the eye homogenate. The BCA protein assay kit was used to estimate the total protein content of the cells and the results of the VEGF protein valuation were adjusted to total protein. Sample absorbance was measured at 450 nm and 550 nm, and the difference was noted[58].

Statistical analysis

The trials were done three times in parallel, unless otherwise noted. GraphPad Prism 6.0 and Origin 9.0 software were castoff to perform the statistical analysis, and the data were displayed as mean ± SD. The unpaired t-test was used to examine the data, and a $p<0.05$ was believed to be statistically significant[59-63].

RESULTS AND DISCUSSION

Physicochemical characterization

The results of FTIR and DSC of RES alone, RES-PLGA physical mixture, RES-PVA physical mixture and RES nanosuspension have been presented in **Figures 1-2**.

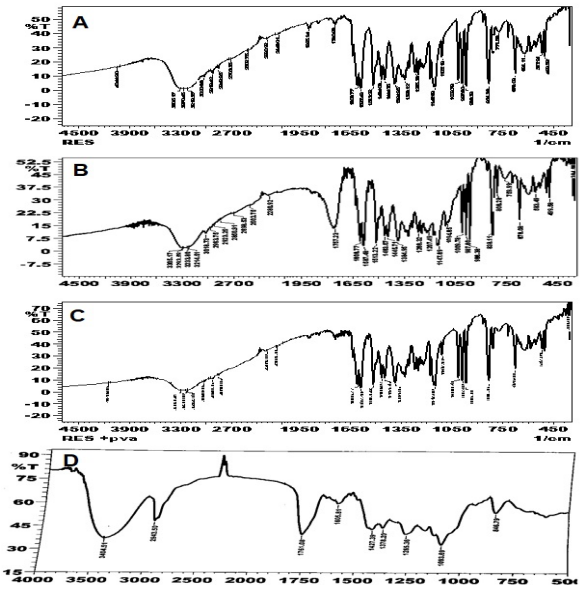

Figure 1: FTIR spectra of RES (A), RES-PLGA Mixture, (B), RES-PVA Mixture (C) and RES Nanosuspension (D)

FTIR was steered to analyse the compatibility of RES with PLGA and to authenticate the RES entrapment in the formulation grounded on results achieved (**Figure 1)**.

FTIR spectrum of RES exhibited peaks between 3200 cm^{-1} and 3400 cm^{-1}, at 1605 cm^{-1}, 1583 cm^{-1}, and 1380 cm^{-1} agreeing to O-H stretching, C=C aromatic double bond stretching, C=C olefinic stretching, and C-C stretching, respectively. The peaks such as 3465 cm^{-1}, 3325 cm^{-1}, 2979-2627 cm^{-1}, 1700-1850 cm^{-1}, and 1050-1250 cm^{-1} approve the existence of O–H, C–H (in $–CH_3$) C–H (in $–CH_2$), –C=O, and C–O groups of PLGA. A reduction in the strength of major peaks of RES and broadening of the peaks was detected in spectrum of RES-PLGA physical mixture simultaneously retaining the characteristic peak. However, no specific peak relating to RES was found in the FTIR spectrum of RES nanosuspension, validating the actual charging of medication in the formulation.

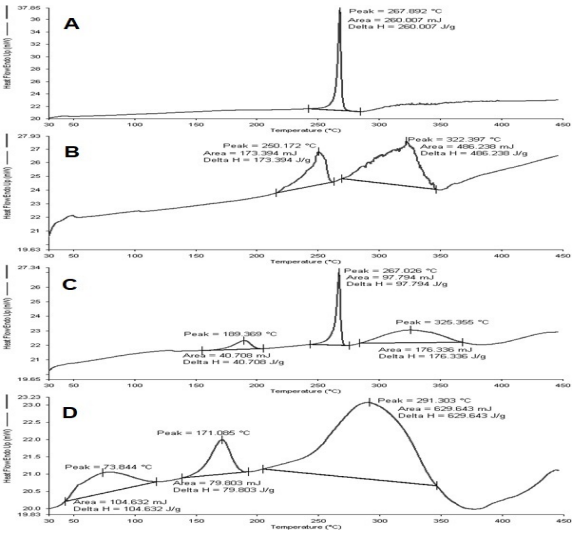

Figure 2: DSC Thermograms of RES (A), RES-PLGA Mixture, (B), RES-PVA Mixture (C) and RES Nanosuspension (D)

To explore the polymer-drug incompatibility, RES alone, RES-PLGA physical mixture, RES-PVA physical mixture and RES nanosuspension were analysed for change in transition temperature on executing DSC (**Figure 2**)[48,64,65]. The acquired DSC thermograms help to ascertain the nature of the drug as well as its physical form in the polymer that can affect drug release profile. Endothermic peak at 267.892°C shown by RES stated its distinctive melting point. DSC thermogram of RES nanosuspension validated RES entrapment in the formulation since the peak at 267.892°C was absent in DSC thermogram of the optimized formulation. Conversely, detection of drug's typical endothermic peak in DSC thermogram of RES-PLGA physical mixture reveals no interaction of RES with either of the two PLGA and PVA. The endothermic peaks obtained from DSC thermograms of RES nanosuspensions indicate the three phase transition temperatures (melting points) of the compounds corresponding to RES, PVA and PLGA. Thus, it could be concluded that the RES nanosuspensions showed three peaks corresponding to. RES, PVA and PLGA.

Optimization of the formulation

To investigate the factors i.e. PLGA and PVA systematically, a CCD was employed (**Table 1** and **Table 2**) with each independent variable at three levels i.e. PLGA at the levels of 30 mg, 40 mg and 50 mg, and PVA at the levels of 1%, 1.5% and 2%. Particle size, PDI and entrapment efficiency were considered as dependent variables[66]. Total 13 formulations were designed using "Design Expert

9.0.4.1" software (Stat-Ease, Minnesota, USA). Two factors at three levels were used entitled Factor 1 i.e. PLGA and Factor 2 i.e. PVA ensuring other ingredients, including drug, constant. To assess the impact of independent variables i.e., factors (PLGA and PVA) on dependent variables i.e., responses (particle size, Y1; PDI, Y2; and entrapment efficiency, Y3), RSM was used (**Table 4**).

Table 4: Observed responses for optimization of RES nanosuspension using central composite design

Std.	Run Order	Factor 1 A: PLGA		Factor 2 B: PVA		Response 1 Particle Size (nm)	Response 2 Poly-dispersity Index	Response 3 Entrapment Efficiency (%)
		Coded Values	Actual Value (mg)	Coded Values	Actual Values (%)			
6	1	+α	54.1421	0	1.5	199.1	0.199	90.31
4	2	+1	50	+1	2	155.2	0.155	72.51
1	3	-1	30	-1	1	180.3	0.181	80.54
2	4	+1	50	-1	1	200.3	0.199	92.35
11	5	0	40	0	1.5	171.2	0.171	71.21
7	6	0	40	-α	0.792893	200.1	0.198	90.5
10	7	0	40	0	1.5	161.1	0.161	75.11
5	8	-α	25.8579	0	1.5	145.2	0.140	75.13
8	9	0	40	+α	2.20711	152.1	0.151	72.17
3	10	-1	30	+1	2	122.4	0.122	75.84
9	11	0	40	0	1.5	151.1	0.154	74.67
13	12	0	40	0	1.5	152.2	0.153	75.43
12	13	0	40	0	1.5	152.9	0.154	75.45

Various models were applied to investigate the combined effects of independent variables i.e. PLGA and PVA on the dependent variable i.e. particle size, PDI and entrapment efficiency. Best fit models were found out on the basis of r^2 and predicted r^2 values (model having largest r^2 value was considered as best fit model). Here, Quadratic Model was observed to be the best fit and is represented by the following mathematical relationship generated using design expert for the studied response variables-

Response = β_0 - β_1 PLGA - β_2 PVA + β_3 PLGA*PVA + β_4 PLGA^2 + β_4 PVA^2 ----3

Five coefficients (β_0 to β_4) were intended signifying β_0 as the intercept, and β_1 to β_4 various quadratic and interaction terms. The equations contain the coefficients for intercept, first-order main effects, interaction terms, and higher-order effects. The sign and the degree of effects indicate the comparative impact of each factor on the response.

Effect of PLGA and PVA on particle size

The results of multiple linear regression analysis are shown by **Equation 4** (r^2 = 0.8990).

Particle Size = 334.22404 – 3.21217 PLGA – 149.99556 PVA + 0.640000 PLGA*PVA + 0.048313 PLGA^2 + 27.22500 PVA^2 ----4

Both the coefficients β1 and β2 bear a negative sign. Negative signs of respective coefficients of PLGA and PVA indicate that on increasing their quantity in the ranges of 25.8579 mg to 54.1421 mg and 0.792893% to 2.20711%, respectively, there will be a significant decrease (p = 0.0022 i.e. <0.05) in particle size. It can be established from **Equation 4** that quantity of PVA is more operational compared with quantity of PLGA as indicated the larger coefficient of PVA than PLGA. The 3D response surface plots and 2D contour plots showing the design space for the effect of PLGA as well as PVA on particle size are presented in **Figure 3**.

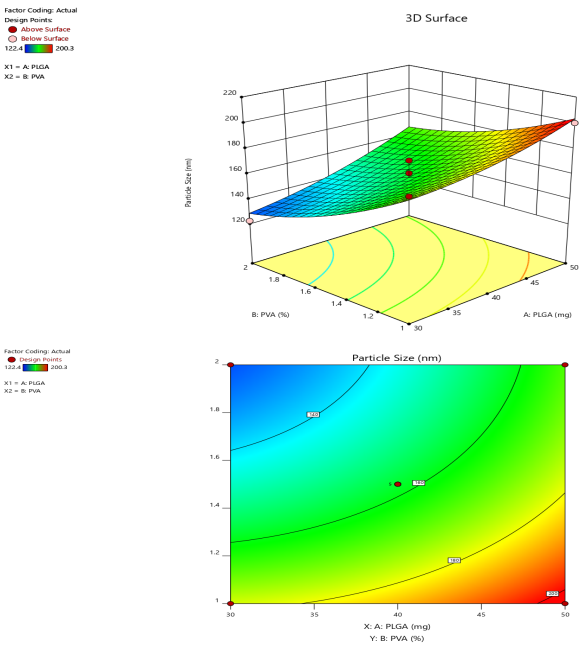

Figure 3. Response Surface Plot (Upper Plot) and Contour Plot (Lower Plot) showing the design space and the effect of PLGA and PVA on particle size

Effect of PLGA and PVA on polydispersity index

The results of multiple linear regression analysis are shown by **Equation 5** (R^2 = 0. 9050).

Polydispersity Index = 0.310244 – 0.002255 PLGA – 0.144517 PVA + 0.000750 PLGA*PVA + 0.000035 PLGA^2 + 0.024050 PVA^2 ----5

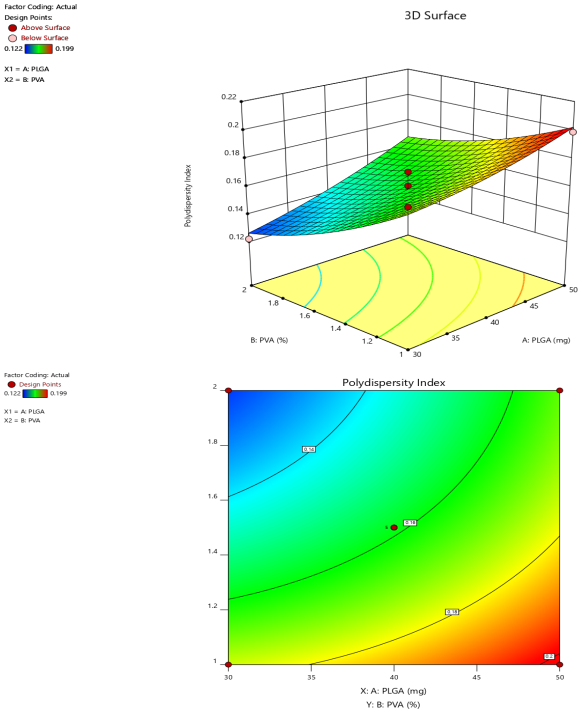

Figure 4. Response Surface Plot (Upper Plot) and Contour Plot (Lower Plot) showing the design space and the effect of PLGA and PVA on PDI

Both coefficients β1 and β2 bear a negative sign. Negative signs of the respective coefficients of PLGA and PVA indicate that on increasing their quantity in the ranges of 25.8579 mg to 54.1421 mg and 0.792893% to 2.20711%, respectively, there will be a major decrease (p = 0.0018 i.e. <0.05) in PDI. It can be established from **Equation 5** that quantity of PVA is more effective compared with quantity of PLGA as indicated the larger coefficient of PVA than PLGA. The 3D response surface plots and 2D contour plots displaying the design space for the effect of PLGA and PVA on PDI are presented in **Figure 4**.

Effect of PLGA and PVA on entrapment efficiency

The results of multiple linear regression analysis are shown by **Equation 6** (R^2 = 0.9403).

Particle Size = 120.26169 – 1.48505 PLGA – 18.94913 PVA - 0.757000 PLGA*PVA + 0.037436 PLGA^2 + 12.20450 PVA^2 ----6

Both coefficients β1 and β2 bear a negative sign. Negative signs of the respective coefficients of PLGA and PVA indicate that on increasing their quantity in the ranges of 25.8579 mg to 54.1421 mg and 0.792893% to 2.20711%, respectively, there will be a significant decrease (p = 0.0004 i.e. <0.05) in entrapment efficiency. It can be established from **Equation 6** that quantity of PVA is more effective compared with quantity of PLGA as indicated the larger coefficient of PVA than PLGA. The 3D response surface plots and 2D contour plots displaying the design space for the effect of PLGA and PVA on entrapment efficiency are presented in **Figure 5**.

Based on the model fitting for each of the response variables, the optimum formulation was chosen by numerical and graphical search techniques. In numerical search, acceptable ranges of the CQAs were defined and weightage assigned for selecting optimized formulation based on the desirability value closer to 1. Based on the ranges of CQAs assigned in numerical search, graphical optimization was performed to demarcate the design space and locating the optimized formulation within the design space.

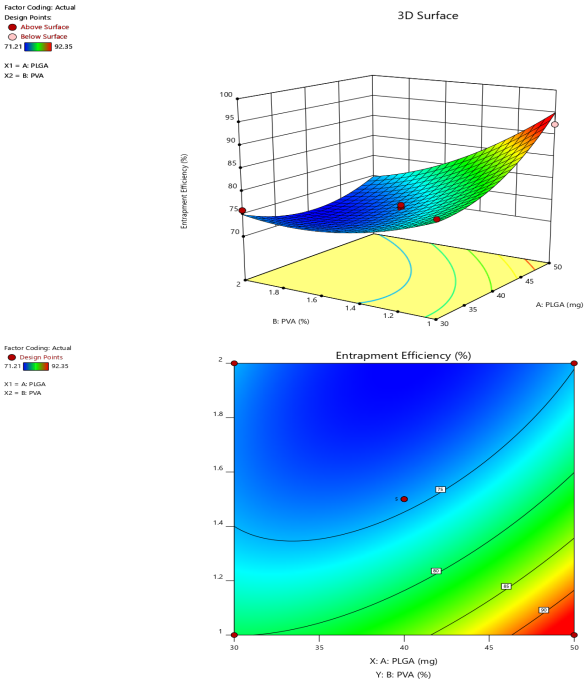

Figure 5. Response Surface Plot (Upper Plot) and Contour Plot (Lower Plot) showing the design space and the effect of PLGA and PVA on entrapment efficiency

During numerical search as well as graphical search (overlay plot, **Figure 6**) methods, 100 solutions were found in the design space having the desirability value of 1 out of which the selected optimized formulation was having PLGA and PVA at the levels of 32.881 mg and 1.329%, correspondingly with response

variables i.e. particle size, PDI and entrapment efficiency values of 157.553 nm, 0.157 and 75.200% respectively.

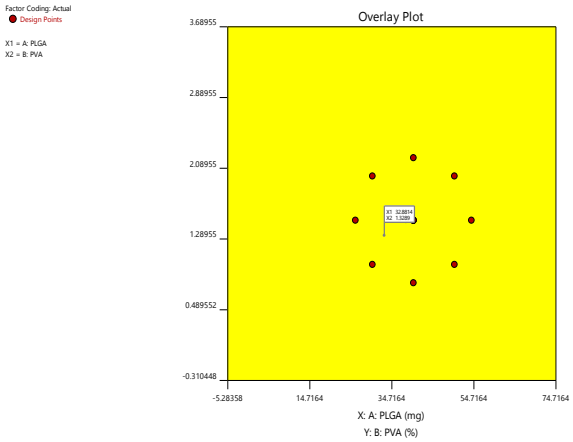

Figure 6. Overlay Plot showing the design space and the selected optimized formulation

Further, RES nanosuspension presented uniform particle size distribution as shown by the low PDI. A "Malvern Zeta Sizer, Nano ZS90", was utilized to assess average zeta potential of RES nanosuspension. A great negative zeta potential of -40.0±4.19 mV confirms the deterrence of particle aggregations and confirms electrostatic stabilization, thus stopping interaction of RES nanosuspension with serum constituents and protein adsorption. This stops the nanoparticles from being up-taken by tissue macrophages[47].

Transmission electron microscopy

The TEM image (**Figure 7**) of optimized formulation showed that the prepared nanosuspension were spherical in shape.

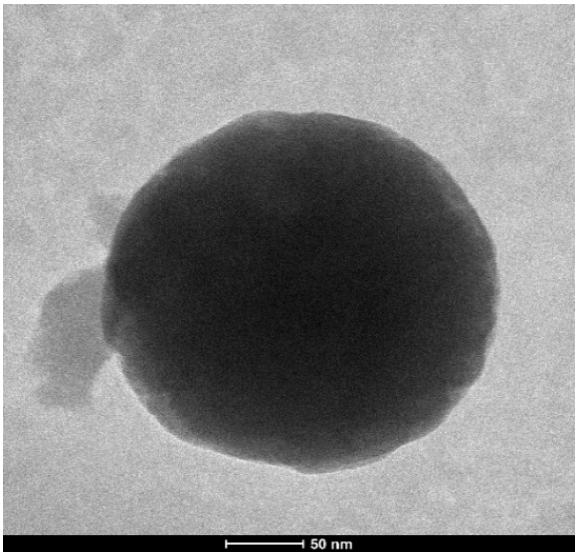

Figure 7. Transmission electron microscopy (TEM) image of the optimized formulation

***In vitro* drug release studies of optimized RES nanosuspension**

In vitro drug release from the optimized RES nanosuspension was made in dialysis bag (12 kDa) using 100 ml of phosphate buffer pH 7.4, i.e. pH of the eye[67], for up to 24 h at 100 RPM and 37 °C ± 0.5 °C temperatures. RES nanosuspension (corresponding to 10 mg RES) was put in dialysis bag and tied on its both ends. Aliquots (2 ml) of samples were withdrawn at pre-set intervals, trailed by replacement with an equivalent bulk of new medium to keep the sink conditions, while drug release was quantified by a suitable validated analytical method. The *in vitro* release data (raw) were analysed by considering volume and drug losses during sampling. The percent drug release was calculated versus time and compared with drug release profile of plain RES (**Table 5, Figure 8**). *In vitro* release behaviour is significant in connecting with the *in vivo* release pattern and formulation behaviour in general[68].

Table 5: *In vitro* drug release profile of the optimized RES nanosuspension and plain RES solution

Time (Hours)	Cumulative Percent Drug Release				
	n1	n2	n3	Average	Standard deviation
1	3.65	4.34	4.28	4.09	0.39
2	5.50	5.66	5.67	5.61	0.09
4	15.79	13.96	17.41	15.72	1.72
6	20.38	21.01	21.09	20.83	0.39
22	67.87	68.92	70.03	68.94	1.08
24	74.54	75.03	72.01	73.86	1.62
28	78.73	78.29	79.35	78.79	0.53
30	81.85	81.54	82.75	82.04	0.63
46	86.86	86.03	85.72	86.20	0.59
48	88.56	89.84	91.08	89.82	1.26

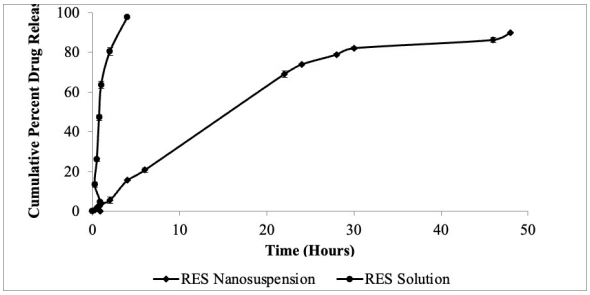

Figure 8: *In vitro* drug release profile of the optimized RES nanosuspension and plain RES solution

To get the drug release mechanism of from RES nanosuspension, the data was handled in several kinetic models i.e. zero-order, first-order, Higuchi and Korsmeyer-Peppas model[69]. The formulation has been found to follow Korsmeyer-Peppas model of drug release i.e. release the drug by non-ficcian transport (**Table 6**).

Table 6: Drug release kinetics data for RES nanosuspension with their respective regression coefficients

Release kinetics	X-axis	Y-axis	R^2	R
Zero order	Time	Cumulative Percent Drug Release	0.9161	0.9571
First-order	Time	Log Cumulative Percent Drug Remaining	0.7485	0.8652
Higuchi	Square Root of Time	Cumulative Percent Drug Release	0.9755	0.9877
Korsmeyer-Peppas	Log Time	Log Cumulative Percent Drug Release	0.9773	0.9886

DPPH antioxidant assay

When DPPH free radical interferes with an odd electron, maximum absorbance was observed at 517 nm (purple color). A free-radical scrounger antioxidant retorts to DPPH to form DPPH-H, which has a minor absorbance when compared to DPPH owing to lesser hydrogen. In contrast to the DPPH-H state that leads to decolourization (yellow hue) due to increase in the number of electrons collected.

It can be seen from **Table 7** that the antioxidant activity of the optimized formulation showed absorbance of 0.511 at 517 nm with the percentage of antioxidant activity as 46.660% with DPPH.

Table 7. DPPH antioxidant assay of the optimized formulation

S. No.	Group	Absorbance at 517 nm	% of Antioxidant Activity
1	Blank (Control)	**0.958**	-
2	RES Nanosuspension	**0.511**	**46.660**
3	RES Solution	**0.654**	**31.733**
4	Ascorbic Acid (Standard)	**0.525**	**45.198**

Age Related Macular Degeneration Studies in Animals

Effect of RES Nanosuspension on Ocular Irritation Test

Rabbits' ocular discomfort was examined under a slit lamp following the administration of different remedies in single doses. The RES nanosuspension did not cause any eye irritation, as evidenced by the absence of redness, swelling, increased secretion, or tears at any point of time and the fact that irritation ratings in all test groups were zero. Additionally, sodium fluorescein was used to further examine the appearance of any corneal damage, and the findings demonstrated that the formulations did not result in corneal damage. The corneal, conjunctival, and retinal tissue of the groups treated with RES nanosuspension and the control group did not vary significantly after fourteen days of continuous treatment. Consequently, ocular tissue was neither irritated nor harmed by the RES nanosuspension.

Assessment of Oxidative Stress

Effect of RES nanosuspension on lipid peroxidation

Compared to the control group, the illness group's ocular homogenate showed increased MDA levels, indicating accelerated lipid peroxidation because of chronic therapy. Long-term administration of bevacizumab (1.25 mg/kg) and free RES (20.0 mg/kg) drastically reduced MDA level ($p<0.01$) in contrast to disease control animals. Moreover, RES-nanosuspension medication (20.0 mg/kg) markedly decreased MDA levels ($p<0.001$). (**Table 8**).

Table 8. Effect of four weeks treatment with resveratrol nanosuspension on lipid peroxidation (MDA) and glutathione level

Group	Treatment (Per kg Body Weight)	Lipid peroxidation (nmol	Glutathione (µmol/mg protein)

		MDA/mg protein)	
Control	Vehicle (1 ml)	1.36 ± 0.16	3.83 ± 0.20
DC	Vehicle (1 ml)	2.53 ± 0.13*	1.74 ± 0.13*
D + RES	Free resveratrol (20.0 mg)	1.79 ± 0.18&	2.51 ± 0.16&
D + RES-NS	Res nanosuspension (20 mg)	1.39 ± 0.17#	3.98 ± 0.18#
D + Bev	Bevacizumab (1.25 mg)	1.68 ± 0.22&	2.43 ± 0.19&

Results are expressed as Mean ± SD.; n = 3 in each group. Data was analysed by one way ANOVA followed by Tukey's multiple comparison test.
Significance: *p< 0.001 when compared with control group; &p< 0.01 when compared with disease control group; #p< 0.001 when compared with disease control group.
Abbreviations: D- disease; DC- disease control; RES- free resveratrol; RES-NS- Resveratrol nanosuspension; Bev- Bevacizumab

Effect of RES nanosuspension on Glutathione

The glutathione levels in the ocular homogenate of diseased animals were markedly lower (p<0.001) than those in the control group. Long-term administration of bevacizumab (1.25 mg/kg) and free RES (20.0 mg/kg) markedly raised glutathione levels (p<0.01) in comparison to disease control animals. Further, RES-nanosuspension therapy (20.0 mg/kg) markedly raised glutathione levels (p<0.001) (**Table 8**).

Effect of RES nanosuspension on Inflammatory Cytokines (TNF-α and IL-6)

After receiving chronic therapy, ocular tissue of the diseased group had higher levels of TNF-α and IL-6 than the control group (p<0.0001). Compared to disease control rabbit, chronic administration of resveratrol (20.0 mg/kg) substantially (p<0.001) reduced TNF-α and IL-1β levels. Furthermore, resveratrol nanosuspension (20.0 mg/kg) and bevacizumab (1.5 mg) reduced TNF-α and IL-1β levels considerably (p<0.0001) when equated to disease control animals after a prolonged period of therapy in rabbit (**Figure 9** and **Figure 10**).

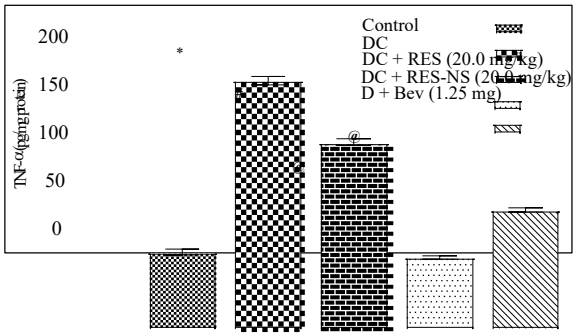

Figure 9. Effect of four weeks treatment with resveratrol nanosuspension on TNF-α levels in eye samples (Mean ± SD, n = 3); Data was analysed by one way ANOVA followed by Tukey's multiple comparison test.
Significance: *p< 0.0001 when compared with control group; #p< 0.01 when compared with disease control group; @p< 0.001 when compared with disease control group.
Abbreviations: D: disease; DC: disease control; RES: free resveratrol; RES-NS: Resveratrol nanosuspension; Bev: Bevacizumab

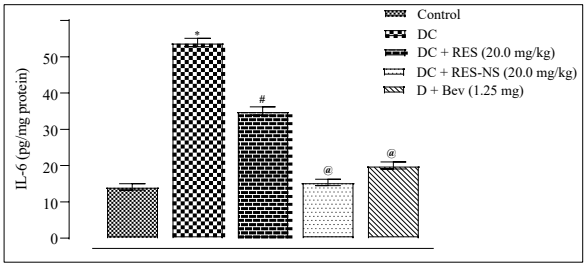

Figure 10. Effect of four weeks treatment with resveratrol nanosuspension on IL6 levels in eye samples (Mean ± SD, n = 3); Data was analysed by one way ANOVA followed by Tukey's multiple comparison test
Significance: *p< 0.0001 when compared with control group; #p< 0.01 when compared with disease control group; @p< 0.001 when compared with disease control group.
Abbreviations: D: disease; DC: disease control; RES: free resveratrol; RES-NS: Resveratrol nanosuspension; Bev: Bevacizumab

Effect of RES nanosuspension treatment on VEGF levels

After receiving chronic treatment, the illness group's eye tissue had higher levels of VEGF than the control group (p<0.0001). When resveratrol (20.0 mg/kg) was administered to rabbit over an extended period of time, VEGF levels were considerably (p<0.001) lower than in disease control rabbit. Furthermore, prolonged administration of bevacizumab (1.5 mg/kg) and

resveratrol nanosuspension (20.0 mg/kg) dramatically ($p<0.0001$) reduced VEGF levels ($p<0.001$) in comparison to disease control rabbit (**Figure 11**).

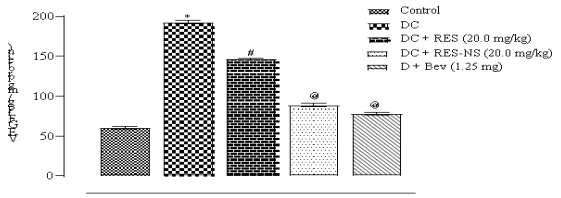

Figure 11. Effect of four weeks treatment with resveratrol nanosuspension on VEGF levels in eye samples

(Mean ± SD, n = 3); Data was analysed by one way ANOVA followed by Tukey's multiple comparison test

Significance: $^{*}p< 0.0001$ when compared with control group; $^{\#}p< 0.01$ when compared with disease control group; $^{@}p< 0.001$ when compared with disease control group.

Abbreviations: D: disease; DC: disease control; RES: free resveratrol; RES-NS: Resveratrol nanosuspension; Bev: Bevacizumab

CONCLUSION

The rational therapy using resveratrol (RES) was developed for the treatment of age-related macular degeneration (AMD). A RES nanosuspension was successfully prepared and optimized using Central Composite Design (CCD). The optimized formulation exhibited an average particle size of 157.55 nm, with a PDI of 0.157 and an entrapment efficiency of 75.20%. In vitro release studies demonstrated sustained ocular delivery, with 89.82% ± 1.26% drug release over 48 hours. The release kinetics followed the Korsmeyer–Peppas model, as indicated by the highest regression coefficient (R^2 = 0.9886), compared to zero-order (0.9571), first-order (0.8652), and Higuchi (0.9877) models. The DPPH assay confirmed that the prepared formulation exhibited strong free radical scavenging activity, comparable to ascorbic acid (standard) and superior to the RES solution. These findings suggest that the developed nanosuspension effectively reduces oxidative stress, a key factor in the pathogenesis of AMD.

ACKNOWLEDGEMENTS

Authors are thankful to Parul University and SGT University for giving the platform to conduct this research work.

ABBREVIATIONS:

AMD: Age-related macular degeneration **DPPH:** 1,1-diphenyl2-picrylhydrazyl; **RES:** Resveratrol; **CCD:** Central Composite Design; **PDI:** Polydisperse Index; **Bev:** Bevacizumab; **MDA:** Malondialdehyde; **RPE:** Retinal Pigment Epithelia; **DLS:** Dynamic light scattering; **DSC:** Differential Scanning Calorimetry; **RSM:** Response Surface Methodology; **VEGF:** Vascular endothelial growth factor; **ROS:** Reactive oxygen species; **TEM:** Transmission Electron Microscopy**;** **GSH:** Glutathione

CONFLICT OF INTERESTS

The authors declare that there is no conflict of interest, financial or otherwise.

FUNDING

Not applicable.

ETHICAL STATEMENT

Applicable.

AUTHORS' CONTRIBUTIONS

Pradeep Kumar Singh: Conceptualization, Methodology, Formal analysis, Data Curation, Resource, Writing - Original Draft.

Komal Patel: Conceptualization, Review & Editing, Visualization, Guidance

Neelkant Prasad: Writing - Review and Editing, Visualization, Resources, Investigation and Validation

Vivek Yadav: Writing - Review & Editing.

REFERENCES

1. Christoforidis JB, Tecce N, Dell'Omo R, Mastropasqua R, Verolino M, Costagliola C. Age related macular degeneration and visual disability. Current Drug Targets. 2011 Feb 1;12(2):221-233. DOI: https://doi.org/10.2174/138945011794182755
2. Ambati J, Ambati BK, Yoo SH, Ianchulev S, Adamis AP. Age-related macular degeneration: etiology, pathogenesis, and therapeutic strategies. Survey of Ophthalmology. 2003 May 1;48(3):257-293. DOI: https://doi.org/10.1016/S0039-6257(03)00030-4.
3. Wong WL, Su X, Li X, Cheung CM, Klein R, Cheng CY, Wong TY. Global prevalence of age-related macular degeneration and disease burden projection for 2020 and 2040: a systematic review and meta-analysis. The Lancet Global Health. 2014 Feb 1;2(2):e106-116. DOI: https://doi.org/10.1016/S2214-109X(13)70145-1.

4. Supuran CT. Agents for the prevention and treatment of age-related macular degeneration and macular edema: a literature and patent review. Expert Opinion on Therapeutic Patents. 2019 Oct 3;29(10):761-767. DOI: https://doi.org/10.1080/13543776.2019.1671353
5. Kang-Mieler JJ, Osswald CR, Mieler WF. Advances in ocular drug delivery: emphasis on the posterior segment. Expert Opinion on Drug Delivery. 2014 Oct 1;11(10):1647-1660. DOI: https://doi.org/10.1517/17425247.2014.935338.
6. Cabrera FJ, Wang DC, Reddy K, Acharya G, Shin CS. Challenges and opportunities for drug delivery to the posterior of the eye. Drug Discovery Today. 2019 Aug 1;24(8):1679-1684. DOI: https://doi.org/10.1016/j.drudis.2019.05.035.
7. Beatty S, Koh HH, Phil M, Henson D, Boulton M. The role of oxidative stress in the pathogenesis of age-related macular degeneration. Survey of Ophthalmology. 2000 Sep 1;45(2):115-134. DOI: https://doi.org/10.1016/S0039-6257(00)00140-5.
8. Abokyi S, To CH, Lam TT, Tse DY. Central role of oxidative stress in age-related macular degeneration: evidence from a review of the molecular mechanisms and animal models. Oxidative Medicine and Cellular Longevity. 2020;2020(1):7901270. DOI: https://doi.org/10.1155/2020/7901270
9. Bungau S, Abdel-Daim MM, Tit DM, Ghanem E, Sato S, Maruyama-Inoue M, Yamane S, Kadonosono K. Health benefits of polyphenols and carotenoids in age-related eye diseases. Oxidative Medicine and Cellular Longevity. 2019;2019(1):9783429. DOI: https://doi.org/10.1155/2019/9783429
10. Xu Z, Sun T, Li W, Sun X. Inhibiting effects of dietary polyphenols on chronic eye diseases. Journal of Functional Foods. 2017 Dec 1;39:186-197. DOI: https://doi.org/10.1016/j.jff.2017.10.031
11. Bhatt P, Fnu G, Bhatia D, Shahid A, Sutariya V. Nanodelivery of resveratrol-loaded PLGA nanoparticles for age-related macular degeneration. AAPS PharmSciTech. 2020 Nov;21:1-9. DOI: https://doi.org/10.1208/s12249-020-01836-4
12. Kasiotis KM, Pratsinis H, Kletsas D, Haroutounian SA. Resveratrol and related stilbenes: their anti-aging and anti-angiogenic properties. Food and Chemical Toxicology. 2013 Nov 1;61:112-120. DOI: https://doi.org/10.1016/j.fct.2013.03.038
13. Kiselev KV. Perspectives for production and application of resveratrol. Applied Microbiology and Biotechnology. 2011 Apr;90:417-425. DOI: https://doi.org/10.1007/s00253-011-3184-8
14. Abu-Amero KK, Kondkar AA, Chalam KV. Resveratrol and ophthalmic diseases. Nutrients. 2016 Apr 5;8(4):200. DOI: https://doi.org/10.3390/nu8040200
15. Rauf A, Imran M, Suleria HA, Ahmad B, Peters DG, Mubarak MS. A comprehensive review of the health perspectives of resveratrol. Food & Function. 2017;8(12):4284-4305. DOI: https://doi.org/10.1039/C7FO01300K
16. King RE, Kent KD, Bomser JA. Resveratrol reduces oxidation and proliferation of human retinal pigment epithelial cells via extracellular signal-regulated kinase inhibition. Chemico-Biological Interactions. 2005 Jan 15;151(2):143-149. DOI: https://doi.org/10.1016/j.cbi.2004.11.003
17. Lee CS, Choi EY, Lee SC, Koh HJ, Lee JH, Chung JH. Resveratrol inhibits hypoxia-induced vascular endothelial growth factor expression and pathological neovascularization. Yonsei Medical Journal. 2015 Nov 1;56(6):1678-1685. DOI: https://doi.org/10.3349/ymj.2015.56.6.1678
18. Xu D, Li Y, Zhang B, Wang Y, Liu Y, Luo Y, Niu W, Dong M, Liu M, Dong H, Zhao P. Resveratrol alleviate hypoxic pulmonary hypertension via anti-inflammation and anti-oxidant pathways in rats. International Journal of Medical Sciences. 2016;13(12):942. DOI: https://doi.org/10.7150/ijms.16810
19. Bryl A, Falkowski M, Zorena K, Mrugacz M. The role of resveratrol in eye diseases—a review of the literature. Nutrients. 2022 Jul 20;14(14):2974. DOI: https://doi.org/10.3390/nu14142974
20. Peng C, Kuang L, Zhao J, Ross AE, Wang Z, Ciolino JB. Bibliometric and visualized analysis of ocular drug delivery from 2001 to 2020. Journal of Controlled Release. 2022 May 1;345:625-645. DOI: https://doi.org/10.1016/j.jconrel.2022.03.031
21. Nayak K, Misra M. A review on recent drug delivery systems for posterior segment of eye. Biomedicine & Pharmacotherapy. 2018 Nov

1;107:1564-1582. DOI: https://doi.org/10.1016/j.biopha.2018.08.138

22. Onoue S, Yamada S, Chan HK. Nanodrugs: pharmacokinetics and safety. International Journal of Nanomedicine. 2014 Feb 20:1025-1037. DOI: http://dx.doi.org/10.2147/IJN.S38378
23. Bezerra MA, Santelli RE, Oliveira EP, Villar LS, LA Escaleira. Response surface methodology (RSM) as a tool for optimization in analytical chemistry. Talanta. 2008; 76(5):965-977. DOI: https://doi.org/10.1016/j.talanta.2008.05.019
24. Mahapatra APK, Saraswat R, Botre M, Paul B, Prasad N. Application of response surface methodology (RSM) in statistical optimization and pharmaceutical characterization of a patient compliance effervescent tablet formulation of an antiepileptic drug levetiracetam. Future Journal of Pharmaceutical Sciences. 2020 Dec;6:1-4. DOI: https://doi.org/10.1186/s43094-020-00096-0
25. Ghosh S, Rao CR (1996) Response surface designs. Design and analysis of experiment Hand book of Statistics, Vol13. Elsevier Sciences B.V, P 343-375. DOI: https://doi.org/10.1016/S0169-7161(96)13013-3
26. Singh B, Chakkal SK, Ahuja N. Formulation and optimization of controlled release mucoadhesive tablets of atenolol using response surface methodology. AAPS Pharm Sci Tech. 2006;7(1):E19-E28. DOI: https://doi.org/10.1208/pt070103
27. Soares LAL, González-Ortega G, Petro-vick PR, Schmidt PC. Optimization of tablets containing a high dose of spray-dried plant extract: a technical note. AAPS Pharm. Sci. Tech. 2005;6(3):E367-371. DOI: https://doi.org/10.1208/pt060346
28. Box GEP, Wilson KB. On the experimental attainment of optimum conditions. Journal of Statistical Royal Society. 1951;13(1): 1-45. DOI: https://doi.org/10.1111/j.2517-6161.1951.tb00067.x
29. Kassem MA, Shaboury KME, Mohammad AI. Application of central composite design for the development and evaluation of chitosan-based colon targeted microspheres and in vitro characterization. Indian J Pharm Sci. 2019;81(2):354-364. DOI: https://doi.org/10.36468/pharmaceutical-sciences.517
30. Bushra R, Shoaib MH, Ali H, Zafar F, Naeem MI, Aslam N, Yousuf RI. Formulation design and optimization of aceclofenac tablets (100 mg) using central composite design with response surface methodology. Lat. Am. J. Pharm. 2014 Jan 1;33(6):1009-1018.
31. Jacob S, Nair AB, Shah J. Emerging role of nanosuspensions in drug delivery systems. Biomaterials research. 2020 Jan 15;24(1):3. DOI: https://doi.org/10.1186/s40824-020-0184-8
32. Ozdemir S, Uner B, Karakucuk A. Resveratrol nanocrystal loaded orodispersible films: Formulation development and in vitro characterization. Research Square. 2021 Sep 14;2021:1-23. DOI: https://doi.org/10.21203/rs.3.rs-873761/v1
33. Bhatt P, Lalani R, Vhora I, Patil S, Amrutiya J, Misra A, Mashru R. Liposomes encapsulating native and cyclodextrin enclosed paclitaxel: Enhanced loading efficiency and its pharmacokinetic evaluation. International journal of pharmaceutics. 2018 Jan 30;536(1):95-107. DOI: https://doi.org/10.1016/j.ijpharm.2017.11.048
34. Yewale C, Baradia D, Patil S, Bhatt P, Amrutiya J, Gandhi R, Kore G, Misra A. Docetaxel loaded immunonanoparticles delivery in EGFR overexpressed breast carcinoma cells. Journal of Drug Delivery Science and Technology. 2018 Jun 1;45:334-345. DOI: https://doi.org/10.1016/j.jddst.2018.03.027.
35. Hasnain MS, Javed MN, Alam MS, Rishishwar P, Rishishwar S, Ali S, Nayak AK, Beg S. Purple heart plant leaves extract-mediated silver nanoparticle synthesis: Optimization by Box-Behnken design. Materials Science and Engineering: C. 2019 Jun 1;99:1105-1114. DOI: https://doi.org/10.1016/j.msec.2019.02.061.
36. Alam MS, Garg A, Pottoo FH, Saifullah MK, Tareq AI, Manzoor O, Mohsin M, Javed MN. Gum ghatti mediated, one pot green synthesis of optimized gold nanoparticles: investigation of process-variables impact using Box-Behnken based statistical design. International journal of biological macromolecules. 2017 Nov 1;104:758-767. DOI: https://doi.org/10.1016/j.ijbiomac.2017.05.129.
37. Alam MS, Javed MN, Pottoo FH, Waziri A, Almalki FA, Hasnain MS, Garg A, Saifullah MK. QbD approached comparison of reaction mechanism in microwave synthesized gold nanoparticles and their superior catalytic role against hazardous nirto-dye. Applied Organometallic Chemistry. 2019

Sep;33(9):e5071.DOI: https://doi.org/10.1002/aoc.5071.

38. Javed MN, Alam MS, Waziri A, Pottoo FH, Yadav AK, Hasnain MS, Almalki FA. QbD applications for the development of nanopharmaceutical products. InPharmaceutical quality by design 2019 Jan 1 (pp. 229-253). Academic Press. DOI: https://doi.org/10.1016/B978-0-12-815799-2.00013-7.
39. Mandal B. *Preparation and physicochemical characterization of Eudragit® RL100 Nanosuspension with potential for Ocular Delivery of Sulfacetamide* (Master's thesis, University of Toledo). DOI: http://rave.ohiolink.edu/etdc/view?acc_num=toledo1271430956.
40. Spek S, Haeuser M, Schaefer MM, Langer K. Characterisation of PEGylated PLGA nanoparticles comparing the nanoparticle bulk to the particle surface using UV/vis spectroscopy, SEC, 1H NMR spectroscopy, and X-ray photoelectron spectroscopy. Applied Surface Science. 2015 Aug 30;347:378-385. DOI: https://doi.org/10.1016/j.apsusc.2015.04.071.
41. Molpeceres J, Aberturas MR, Guzman M. Biodegradable nanoparticles as a delivery system for cyclosporine: preparation and characterization. Journal of microencapsulation. 2000 Jan 1;17(5):599-614. DOI: https://doi.org/10.1080/026520400417658
42. Mujtaba MA, Alotaibi NM, Alshehri SM, Yusuf M, Anwer MK, Rahman MA, Parveen A. Novel therapeutic approach in PEGylated chitosan nanoparticles of Apigenin for the treatment of cancer via oral nanomedicine. Polymers. 2022 Oct 15;14(20):4344. DOI: https://doi.org/10.3390/polym14204344
43. Garg S, Patel P, Gupta GD, Kurmi BD. Pharmaceutical applications and advances with zetasizer: an essential analytical tool for size and zeta potential analysis. Micro and Nanosystems. 2024 Sep 1;16(3):139-154. DOI: https://doi.org/10.2174/0118764029301470240603051432
44. Zhou Q, Liu L, Zhang D, Fan X. Preparation and characterization of gemcitabine liposome injections. Die Pharmazie-An International Journal of Pharmaceutical Sciences. 2012 Oct 1;67(10):844-847. DOI: https://doi.org/10.1691/ph.2012.1157
45. Chung S, Yao H, Caito S, Hwang JW, Arunachalam G, Rahman I. Regulation of SIRT1 in cellular functions: role of polyphenols. Archives of biochemistry and biophysics. 2010 Sep 1;501(1):79-90. DOI: https://doi.org/10.1016/j.abb.2010.05.003
46. Zhang C, Qineng P, Zhang H. Self-assembly and characterization of paclitaxel-loaded N-octyl-O-sulfate chitosan micellar system. Colloids and Surfaces B: Biointerfaces. 2004 Nov 25;39(1-2):69-75. DOI: https://doi.org/10.1016/j.colsurfb.2004.09.002
47. Valko M, Leibfritz D, Moncol J, Cronin MT, Mazur M, Telser J. Free radicals and antioxidants in normal physiological functions and human disease. The international journal of biochemistry & cell biology. 2007 Jan 1;39(1):44-84. DOI: https://doi.org/10.1016/j.biocel.2006.07.001
48. Alshetaili AS, Anwer MK, Alshahrani SM, Alalaiwe A, Alsulays BB, Ansari MJ, Imam F, Alshehri S. Characteristics and anticancer properties of Sunitinib malate-loaded poly-lactic-co-glycolic acid nanoparticles against human colon cancer HT-29 cells lines. Tropical Journal of Pharmaceutical Research. 2018;17(7):1263-1269. DOI: https://doi.org/10.4314/tjpr.v17i7.6.
49. Jung JW, Yoon BH, Oh HR, Ahn JH, Kim SY, Park SY, Ryu JH. Anxiolytic-like effects of Gastrodia elata and its phenolic constituents in mice. Biological and Pharmaceutical Bulletin. 2006;29(2):261-265. DOI: https://doi.org/10.1248/bpb.29.261
50. Zhou P, Kannan R, Spee C, et al. Protection of retina by alphaB crystallin in sodium iodate induced retinal degeneration. PLoS One. 2014;9(5):e98275. DOI: https://doi.org/10.1371/journal.pone.0098275
51. Bhatt P, Fnu G, Bhatia D, Shahid A, Sutariya V. Nanodelivery of Resveratrol-Loaded PLGA Nanoparticles for Age-Related Macular Degeneration. AAPS PharmSciTech 2020;21(8):291. DOI: https://doi.org/10.1208/s12249-020-01836-4
52. Morsi N, Ibrahim M, Refai H, et al. Nanoemulsion-based electrolyte triggered in situ gel for ocular delivery of acetazolamide. Eur J Pharm Sci 2017;104:302-314. DOI: https://doi.org/10.1016/j.ejps.2017.04.013
53. Ohkawa H, Ohishi N, Yagi K. Assay for lipid peroxides in animal tissues by thiobarbituric acid reaction. Anal Biochem 1979;95(2):351-358.

DOI: https://doi.org/10.1016/0003-2697(79)90738-3

54. Tsikas D, Rothmann S, Schneider JY, Suchy MT, Trettin A, Modun D, Stuke N, Maassen N, Frölich JC. Development, validation and biomedical applications of stable-isotope dilution GC–MS and GC–MS/MS techniques for circulating malondialdehyde (MDA) after pentafluorobenzyl bromide derivatization: MDA as a biomarker of oxidative stress and its relation to 15 (S)-8-iso-prostaglandin F2α and nitric oxide (NO). Journal of Chromatography B. 2016 Apr 15;1019:95-111. DOI: https://doi.org/10.1016/j.jchromb.2015.10.009.
55. Ellman GL. Tissue sulfhydryl groups. Arch Biochem Biophys 1959;82:70-77.
56. Sattar AA, Matin AA, Hadwan MH, Hadwan AM, Mohammed RM. Rapid and effective protocol to measure glutathione peroxidase activity. Bulletin of the National Research Centre. 2024 Oct 8;48(1):100. DOI: https://doi.org/10.1186/s42269-024-01250-x.
57. Rajput MS, Sarkar PD. Modulation of neuro-inflammatory condition, acetylcholinesterase and antioxidant levels by genistein attenuates diabetes associated cognitive decline in mice. Chemico-Biological Interactions 2017;268(1):93-102. DOI: https://doi.org/10.1016/j.cbi.2017.02.021
58. Takahashi H, Nomura Y, Nishida J, Fujino Y, Yanagi Y, Kawashima H. Vascular Endothelial Growth Factor (VEGF) Concentration Is Underestimated by Enzyme-Linked Immunosorbent Assay in the Presence of Anti-VEGF Drugs. *Invest Ophthalmol Vis Sci*. 2016;57(2):462-466. DOI: https://doi.org/10.1167/iovs.15-18245
59. Shang Q, Zhai J, Tian R, Zheng T, Zhang X, Liang X, Zhang J. Fabrication, characterization, and controlled release of eprinomectin from injectable mesoporous PLGA microspheres. RSC advances. 2015;5(92):75025-32. DOI: https://doi.org/10.1039/C5RA12262G
60. Hoare TR, Kohane DS. Hydrogels in drug delivery: Progress and challenges. polymer. 2008 Apr 15;49(8):1993-2007. DOI: https://doi.org/10.1016/j.polymer.2008.01.027
61. Sadat SM, Jahan ST, Haddadi A. Effects of size and surface charge of polymeric nanoparticles on in vitro and in vivo applications. Journal of Biomaterials and Nanobiotechnology. 2016;7(02):91-108. DOI: http://dx.doi.org/10.4236/jbnb.2016.72011
62. Huo M, Zhao Y, Satterlee AB, Wang Y, Xu Y, Huang L. Tumor-targeted delivery of sunitinib base enhances vaccine therapy for advanced melanoma by remodeling the tumor microenvironment. Journal of Controlled Release. 2017 Jan 10;245:81-94. DOI: https://doi.org/10.1016/j.jconrel.2016.11.013
63. Misra A, Shahiwala A, editors. *In-vitro* and *in-vivo* tools in drug delivery research for optimum clinical outcomes. CRC Press; 2018 Jun 22. DOI:. https://doi.org/10.1201/b22448
64. Askarizadeh M, Esfandiari N, Honarvar B, Sajadian SA, Azdarpour A. Kinetic modeling to explain the release of medicine from drug delivery systems. ChemBioEng Reviews. 2023 Dec;10(6):1006-1049. DOI: https://doi.org/10.1002/cben.202300027
65. Kobierski S, Ofori-Kwakye K, Müller RH, Keck CM. Resveratrol nanosuspensions for dermal application–production, characterization, and physical stability. Die Pharmazie-An International Journal of Pharmaceutical Sciences. 2009 Nov 1;64(11):741-747. DOI: https://doi.org/10.1691/ph.2009.9097
66. Javed MN, Pottoo FH, Shamim A, Hasnain MS, Alam MS. Design of experiments for the development of nanoparticles, nanomaterials, and nanocomposites. In Design of Experiments for Pharmaceutical Product Development: Volume II: Applications and Practical Case studies 2021 Jan 23 (pp. 151-169). Singapore: Springer Singapore. DOI: https://doi.org/10.1007/978-981-33-4351-1_9
67. Abdelrahman AA, Salem HF, Khallaf RA, Ali AM. Modeling, optimization, and in vitro corneal permeation of chitosan-lomefloxacin HCl nanosuspension intended for ophthalmic delivery. Journal of pharmaceutical innovation. 2015 Sep;10(3):254-268. DOI: https://doi.org/10.1007/s12247-015-9224-7.
68. Du Toit LC, Carmichael T, Govender T, Kumar P, Choonara YE, Pillay V. In vitro, in vivo, and in silico evaluation of the bioresponsive behavior of an intelligent intraocular implant. Pharmaceutical research. 2014 Mar;31(3):607-634. https://doi.org/10.1007/s11095-013-1184-3
69. Askarizadeh, M., Esfandiari, N., Honarvar, B., Sajadian, S.A. and Azdarpour, A. Kinetic Modeling to Explain the Release of Medicine

from Drug Delivery Systems. CBEN, 2023;10: 1006-1049. DOI: https://doi.org/10.1002/cben.202300027